

000  
001  
002  
003  
004  
005  
006  
007  
008  
009  
010  
011  
012  
013  
014  
015054  
055  
056  
057  
058  
059  
060  
061  
062  
063  
064  
065  
066  
067  
068  
069  
070  
071  
072  
073  
074  
075  
076  
077  
078  
079  
080  
081  
082  
083  
084  
085  
086  
087  
088  
089  
090  
091  
092  
093  
094  
095  
096  
097  
098  
099  
100  
101  
102  
103  
104  
105  
106  
107

# External Patch Group Prior Guided Internal Orthogonal Dictionary Learning for Real Image Denoising

Anonymous CVPR submission

Paper ID \*\*\*\*

## Abstract

For image denoising problem, the external and internal priors are playing key roles in many different methods. External priors learn from external images to restore noisy images while internal ones exploit priors of given images for denoising. The external priors are more generative and efficient on recovering structures existing in most images while the internal priors are more adaptive on recovering details existed in given noisy images. In this paper, we propose to employ the external patch group prior of images to guide the clustering of internal patch groups, and develop an external dictionary guided internal orthogonal dictionary learning algorithm for real image denoising. The internal orthogonal dictionary learning process has closed-form solutions and hence very efficient for online denoising. The experiments on standard datasets demonstrate that, that the proposed method achieves much better denoising performance than the other state-of-the-art methods on real image denoising.

## 1. Introduction

Most vision systems, such as medical imaging and surveillance, need accurate feature extraction from high-quality images. The camera sensors and outdoor low light conditions will unavoidly bring noise to the captured images. The impact is that the image details will be lost or hardly visible. As a result, image denoising is an essential procedure for the reliability of these vision systems. In the research area, image denoising is also an ideal platform for testing natural image models and provides high-quality images for other computer vision tasks such as image registration, segmentation, and pattern recognition, etc.

For several decades, there emerge numerous image denoising methods [1, 2, 3, 4, 5, 6, 7, 8, 9, 10, 11], and all of them focus mainly on dealing with additive white Gaussian noise (AWGN). In real world, the cameras will undertake high ISO settings for high-speed shots on actions,

long exposure for low light on night shots, etc. Under these situations, the noise is generated in a complex form and also been changed during the in-camera imaging pipeline [12, 13]. Therefore, the noise in real images are much more complex than Gaussian [13, 24]. It depends on camera series, brands, as well as the settings (ISO, shutter speed, and aperture, etc). The models designed for AWGN would become much less effective on real noisy images.

In the last decade, the methods of [14, 15, 16, 17, 18, 19, 13] are developed to deal with real noisy images. Almost all these methods employ a two-stage framework: estimating the parameters of the assumed noise model (usually Gaussian) and performing denoising with the help of the noise modeling and estimation in the first stage. However, the Gaussian assumption is inflexible in describing the complex noise on real noisy images [16]. Although the mixture of Gaussians (MoG) model is possible to approximate any noise distribution [20], estimating its parameters is time consuming via nonparametric Bayesian techniques [19]. To evaluate the performance of these methods on dealing with complex real noise, we apply these methods, with corresponding default parameters, on a real noisy image provided in [13]. The testing image is captured by a Nikon D800 camera when ISO is 3200. The "ground truth" image is also provided with which we can calculate objective measurements such as PSNR and SSIM [21]. The denoised images are listed in Figure 1, from which we can see that these methods either remove the noise or oversmooth the complex details in real noisy image.

The above mentioned methods can be categorized into external methods which learn priors from external images to recover noisy images, and internal ones which exploit priors of given images for denoising. The external priors in natural images are free of the high correlation between noise and signals in real noisy images, while the internal prior is adaptive to the image and can recover better the latent clean image. Combining the priors of external clean images and adaptively of internal testing images can naturally improve the performance of denoising methods, especially on real noisy images. Based on these observations, in this paper,

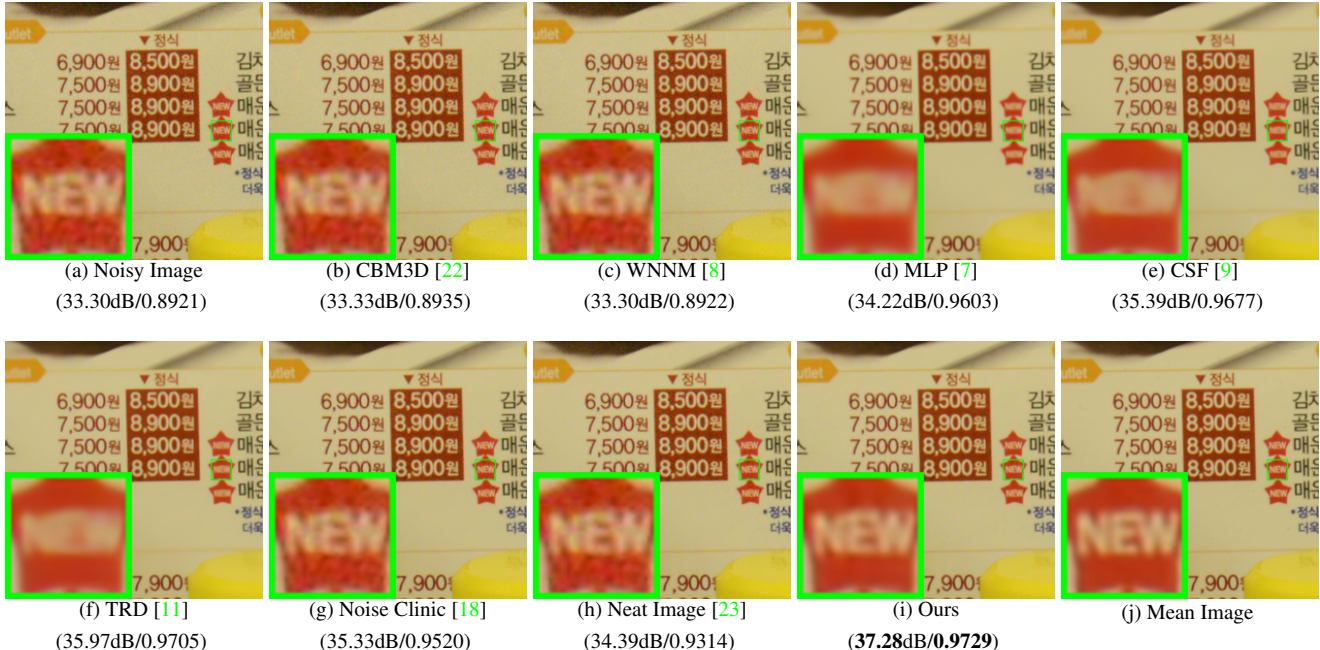


Figure 1. Denoised images of the real noisy image “*NikonD800ISO3200A3*” by different methods. The images are better to be zoomed on screen.

we propose to employ the external patch group prior [10] of natural clean images to guide the clustering of internal patch groups in given noisy image, and develop an external prior guided internal orthogonal dictionary learning (DL) algorithm for real image denoising. The internal orthogonal DL process includes two alternating stages: updating sparse coefficients and updating orthogonal dictionary. Both of the two stages have closed-form solutions. Hence, our internal DL process is very efficient for online internal denoising. Through comprehensive experiments on real noisy images captured by different cameras and settings, we demonstrate that the proposed method achieves better performance on real image denoising.

## 1.1. Our Contributions

The contributions of this paper are summarized as follows:

- We propose a novel dictionary learning method which employ the external prior guided the internal orthogonal dictionary learning for real image denoising. Both the external prior and internal prior are performed on patch groups instead of patches.
- The internal orthogonal dictionary learning are alternating iterative solved with closed-form solutions. The learned orthogonal dictionary are very efficient in both learning and denoising stages.
- We achieve much better performance on the real image

denoising problem than other competing methods in terms of visual quality, PSNR, and SSIM.

The rest of this paper will be summarized as follows: in Section 2, we will introduce the related work; in Section 3, we will introduce the proposed external prior guided internal orthogonal dictionary learning algorithm for real image denoising; in Section 4, we will demonstrate the extensive experiments on two standard dataset; we will conclude our paper and give our future work in Section 5.

## 2. Related Work

### 2.1. Patch Group Prior of Natural Images

The Patch Group (PG) prior [10] is proposed to directly model the non-local self similar (NSS) property of natural images. The NSS property is commonly used in image restoration tasks [1, 4, 5, 8, 10]. The PG prior largely reduces the space of images to be modeled when compared to the patch prior [6]. The better modeling on NSS is demonstrated via better image denoising performance on natural images. However, in [10], only the PGs of clean natural images is utilized, while the PGs of noisy input images are ignored. In this paper, we aim at making use of both PGs from natural clean images and real noisy images for better denoising performance.

### 2.2. Internal v.s. External Dictionary Learning

For natural images, the internal patch recurrence across multiple scales has been successfully applied in many

image restoration problems [25, 26, 27, 28]. These work demonstrate that internal information is enough for many ill-posed problems including denoising additive white Gaussian noise. The rationale is, since the AWGN noise is independent of the original clean images, it will be reduced if the image is scaled to a smaller size. However, the noise in real images is generated mostly from the camera sensors, which is highly complex and signal dependent [13]. Besides, according to the seminar workd of [24], the noise in real images has fixed patterns from several main sources. Therefore, we can hardly seperate the complex noise from the signals without the help of external (correct) information of natural clean images. Only using the internal information may be not enough for real image denoising problem. On the other hand, the methods only using the external information may be not adaptive for real noisy images. Recently, the methods of [7, 9, 11] had been proposed to learn, on both internal and external images, a process directly mapping the noisy patches to denoised ones. These discriminative learning based methods are only effective on additive white Gaussian noise and ineffective on complex and signal dependent noise in real images. This has been shown in Figure 1. In this paper, our goal is to make use of external information to guide the subspace learning of internal PGs for image denoising task.

### 2.3. Real Image Denoising

To the best of our knowledge, the study of real image denoising can be dated back to the BLS-GSM model [29], in which Portilla et al. proposed to use scale mixture of Gaussian in overcomplete oriented pyramids to estimate the latent clean images. In [14], Portilla proposed to use a correlated Gaussian model for noise estimation of each wavelet subband. Based on the robust statistics theory [30], the work of Rabie [15] modeled the noisy pixels as outliers, which could be removed via Lorentzian robust estimator. In [16], Liu et al. proposed to use 'noise level function' (NLF) to estimate the noise and then use Gaussian conditional random field to obtain the latent clean image. Recently, Gong et al. proposed an optimization based method [17], which models the data fitting term by weighted sum of  $\ell_1$  and  $\ell_2$  norms and the regularization term by sparsity prior in the wavelet transform domain. Later, Lebrun el al. proposed a multiscale denoising algorithm called 'Noise Clinic' [18] for real image denoising task. This method generalizes the NL-Bayes [31] to deal with signal, scale, and frequency dependent noise. Recently, Zhu et al. proposed a Bayesian model [19] which approximates the noise via Mixture of Gaussian (MoG) model [20]. The clean image is recovered from the noisy image by the proposed Low Rank MoG filter (LR-MoG). In this paper, we proposed a noval denoising method achieving much better performance than previous real denoising methods.

## 3. External Patch Group Prior Guided Internal Orthogonal Dictionary Learning

In this section, we formulate the framework of external Patch Group prior guided internal subspace learning. We first introduce the patch group prior leaning on clean natural RGB images. Then we formulate the external guided internal subspace learning. Finally, we discuss the differences between external subspaces and the corresponding internal subspace.

### 3.1. External Patch Group Prior Learning

Natural images often demonstrate repetitive patterns, this nonlocal self-similarity (NSS) property is a key successful factor for many image denoising methods [1, 4, 5, 32, 8, 10] and restoration methods [ ]. In [10], the NSS property is directly learned as an external prior in a patch group manner. In this section, we formulate the Patch Group prior on natural color images.

In [10], the patch group (PG) is defined as a group of similar patches to the local patch. The patch group mean is distracted, and hence different groups patches can share similar PGs. Therefore the space to be modeled is largely reduced. In this work, we extract PGs from RGB images. Each patch is of size  $p \times p \times 3$ . For each local patch, we search its similar patches around it through the Euclidean distance in a local window of size  $W \times W$ . The PG is denoted by  $\{\mathbf{x}_m\}_{m=1}^M$ , where  $\mathbf{x}_m \in \mathbb{R}^{3p^2 \times 1}$  is a color image patch vector. The mean vector of this PG is  $\boldsymbol{\mu} = \frac{1}{M} \sum_{m=1}^M \mathbf{x}_m$ , and  $\bar{\mathbf{x}}_m = \mathbf{x}_m - \boldsymbol{\mu}$  is the group mean subtracted patch vector. The PG is defined as  $\bar{\mathbf{X}} \triangleq \{\bar{\mathbf{x}}_m\}, m = 1, \dots, M$ , and it represent the external NSS prior on color images. Assume we have extracted  $N$  PGs from a given set of natural images, and the  $n$ -th PG is defined as  $\bar{\mathbf{X}}_n \triangleq \{\bar{\mathbf{x}}_{n,m}\}_{m=1}^M, n = 1, \dots, N$ . We employ the patch group based Gaussian Mixture Model (PG-GMM) for NSS prior learning. We aim to learn a set of  $K$  Gaussians  $\{\mathcal{N}(\boldsymbol{\mu}_k, \Sigma_k)\}$  from  $N$  training PGs  $\{\bar{\mathbf{X}}_n\}$ , while requiring that all the  $M$  patches  $\{\bar{\mathbf{x}}_{n,m}\}$  in PG  $\bar{\mathbf{X}}_n$  belong to the same Gaussian component and assume that the patches in the PG are independently sampled. Note that such an assumption is commonly used in patch based image modeling [3, 5]. Then, the likelihood of  $\{\bar{\mathbf{X}}_n\}$  can be calculated as

$$P(\bar{\mathbf{X}}_n) = \sum_{k=1}^K \pi_k \prod_{m=1}^M \mathcal{N}(\bar{\mathbf{x}}_{n,m} | \boldsymbol{\mu}_k, \Sigma_k). \quad (1)$$

By assuming that all the PGs are independently sampled, the overall objective log-likelihood function is

$$\ln \mathcal{L} = \sum_{n=1}^N \ln \left( \sum_{k=1}^K \pi_k \prod_{m=1}^M \mathcal{N}(\bar{\mathbf{x}}_{n,m} | \boldsymbol{\mu}_k, \Sigma_k) \right). \quad (2)$$

We maximize the above objective function for PG-GMM learning and finally obtain the GMM model with learned parameters including mixture weights  $\{\pi_k\}_{k=1}^K$ , mean vectors

324      $\{\mu_k = \mathbf{0}\}_{k=1}^K$ , and covariance matrices  $\{\Sigma_k\}_{k=1}^K$ . Noted  
 325     that the mean vector of each cluster is natural zeros, i.e.,  
 326      $\mu_k = \mathbf{0}$ .

### 328     3.2. External Prior Guided Internal Orthogonal 329         Dictionary Learning

330     Given a rael noisy image, we extract noisy PGs from it  
 331     and save the mean vectors of each PG for recovering. The  
 332     mean substracted PG is defined as  $\bar{\mathbf{Y}}$ . To project this PG  
 333     into a most adaptive subspace, we select the most suitable  
 334     Gaussian component to it from the PG-GMM trained in pre-  
 335     vious section. The selection can be done by checking the  
 336     posterior probability that  $\bar{\mathbf{Y}}$  belongs to the  $k$ th Gaussian  
 337     component:

$$339 \quad P(k|\bar{\mathbf{Y}}) = \frac{\prod_{m=1}^M \mathcal{N}(\bar{\mathbf{y}}_m | \mathbf{0}, \Sigma_k)}{\sum_{l=1}^K \prod_{m=1}^M \mathcal{N}(\bar{\mathbf{y}}_m | \mathbf{0}, \Sigma_l)}. \quad (3)$$

342     Since the noise on real images are mostly small when com-  
 343     pared to the signals, the covariance matrix of the  $k$ th com-  
 344     ponent is still  $\Sigma_k$ . Finally, the component with the maxi-  
 345     mum A-posteriori (MAP) probability  $\ln P(k|\bar{\mathbf{Y}})$  is selected  
 346     as the most suitable subspace for  $\bar{\mathbf{Y}}$ .

347     Though each PG has been projected into its most suitable  
 348     subspace, the pre-learned subspace is still too general to  
 349     represent the noisy PG extracted from the real noisy image.  
 350     That is, the noisy PGs projected into one cluster can still  
 351     constisted a subspace which is of lower dimensions than the  
 352     subspace pre-learned from the external PGs. This can be  
 353     demonstrated by compare the distribution of external PGs  
 354     and internal PGs in the same clusters. We randomly select  
 355     one cluster, and collect the celan PGs extracted from exter-  
 356     nal dataset (Kodak 24 images) and the niosy PGs from the  
 357     testing image. Since the original PGs are of  $3p^2$  dimensions,  
 358     we apply PCA to project the PGs into 2 dimensions for bet-  
 359     ter visualization. The results is shown in Figure ??, from  
 360     which we can see clearly that the projected PGs are mainly  
 361     in a smaller region of the external PGs, which proves that  
 362     the internal PGs are only consisted a subspace in a lower  
 363     dimension than the PGs collected from external subspace.  
 364     To better and adaptively charactering the internal PGs from  
 365     the testing image, we need learn a more specific dictionary  
 366     for noisy PGs assigned into each cluster. For notation sim-  
 367     plicity, we ignore the index of subspace  $k$ . The internal PGs  
 368      $\mathbf{Y}$  form a subspace which can be obtained by singular value  
 369     decomposition (SVD),

$$370 \quad \min_{\mathbf{D}_i \in \mathbb{R}^{3p^2 \times r}, \mathbf{A} \in \mathbb{R}^{3p^2 \times MN}} \|\mathbf{Y} - [\mathbf{D}_e \mathbf{D}_i] \mathbf{A}\|_F^2 + \lambda \|\mathbf{A}\|_1 \\ 371 \quad \text{s.t. } \mathbf{D}_i^T \mathbf{D}_i = \mathbf{I}_r, \mathbf{D}_e^T \mathbf{D}_i = \mathbf{0}, \quad (4)$$

374     The singular vectors capture the statistical structures of NSS  
 375     variations in natural images, while the singular values in  $\mathbf{S}$   
 376     represent the significance of these singular vectors. Fig. 4  
 377     shows the singular vectors for one Gaussian component.

### 378     3.3. Optimization with Closed-form Solution

379     Similar to the K-SVD [3], we employ an alternating it-  
 380     erative framework to solve the optimization problem 4. In  
 381     fact, we initialize the orthogonal dictionary as  $\mathbf{D}^{(0)}$  and for  
 382      $t = 0, 1, \dots, T - 1$ , alternatively do

383         **Updating Sparse Coefficients:** given the initialization  
 384         orthogonal dictioanry  $\mathbf{D}_i^{(t)}$ , the sparce coefficients  $\mathbf{A}^{(t)}$  are  
 385         obtained via solving

$$386 \quad \mathbf{A}^{(t)} := \arg \min_{\mathbf{A} \in \mathbb{R}^{3p^2 \times MN}} \|\mathbf{Y} - [\mathbf{D}_e \mathbf{D}_i^{(t)}] \mathbf{A}\|_F^2 + \lambda \|\mathbf{A}\|_1. \quad (5)$$

387     This problem has closed-form solution by  $\mathbf{A}^* = T_\lambda(\hat{\mathbf{D}}^T \mathbf{Y})$ , where  $T_\lambda(\mathbf{A}) = \text{sgn}(\mathbf{A}) \odot \max(\mathbf{A}, \lambda)$  is a soft-  
 388     thresholding function.

389         **Updating Orthogonal Dictionary:** given the sparse co-  
 390         efficients  $\mathbf{A}^{(0)}$ , the sparce coefficients  $\mathbf{A}^{(t)}$  are obtained via  
 391         solving

$$392 \quad \mathbf{D}_i^{(t+1)} := \arg \min_{\mathbf{D}_i \in \mathbb{R}^{3p^2 \times r}} \|\mathbf{Y} - [\mathbf{D}_e \mathbf{D}_i] \mathbf{A}^{(t)}\|_F^2 \\ 393 \quad \text{s.t. } \mathbf{D}_i^T \mathbf{D}_i = \mathbf{I}_r, \mathbf{D}_e^T \mathbf{D}_i = \mathbf{0}, \quad (6)$$

394     Dividing the sparse coefficients  $\mathbf{A} = [\mathbf{A}_e^T \mathbf{A}_i^T]^T$ , where  $\mathbf{A}_e$   
 395     and  $\mathbf{A}_i$  denote the coefficients over external and internal  
 396     dictionary  $\mathbf{D}_e$  and  $\mathbf{D}_i$ . According to the Proposition 2.2  
 397     in [33], the problem (6) has a closed-form solution  $\mathbf{D}_i^* = \mathbf{U} \mathbf{V}^T$ , where  $\mathbf{U}$  and  $\mathbf{V}$  are the orthogonal matrices obtained  
 398     by the following SVD

$$399 \quad (\mathbf{I} - \mathbf{D}_e \mathbf{D}_e^T) \mathbf{Y} \mathbf{A}_i^T = \mathbf{U} \Sigma \mathbf{V}^T \quad (7)$$

400     With these solutions, the final obtained dictionary  $\mathbf{D} = [ \mathbf{D}_e \mathbf{D}_i ]$  are orthogonal ictionary. This can be proved by  
 401     the following equation

$$402 \quad \mathbf{D}^T \mathbf{D} = \begin{pmatrix} \mathbf{D}_e^T \\ \mathbf{D}_i^T \end{pmatrix} (\mathbf{D}_e \mathbf{D}_i) = \begin{pmatrix} \mathbf{D}_e^T \mathbf{D}_e & \mathbf{D}_e^T \mathbf{D}_i \\ \mathbf{D}_i^T \mathbf{D}_e & \mathbf{D}_i^T \mathbf{D}_i \end{pmatrix} = \mathbf{I} \quad (8)$$

### 413     3.4. Discussion on External Prior and Internal Or- 414         thogonal Dictionary Learning

415     Until now, we have divided the noisy PGs into multiple  
 416     internal subspaces. Here we take a deep analysis on how the  
 417     external NSS prior guide the subspace learning of internal  
 418     PGs. The help are at least threefold. Firstly, through MAP  
 419     in (3), the external prior guides the noisy PGs to be clustered  
 420     into the correct subspaces. If we cluster the noisy PGs in an  
 421     automatical way, the subspaces we learned will be highly  
 422     degraded by the signal dependent noise. Secondly, the guid-  
 423     ance of external prior for internal clustering is more efficient  
 424     than directly clustering the internal noisy PGs. It only needs  
 425     to calculate the MAP probability via the equation (3) while  
 426     the internal clustering via GMM is time-consuming on EM

432 algorithm [34]. Thirdly, due to the correct guidance of external prior, the structural decomposition via SVD of each  
 433 subspace is more adaptive. This will bring better denoising performance than the methods only using the external  
 434 information. The *mutual incoherence*  $\mu(\mathbf{U})$  [35], which is  
 435 defined as

$$\mu(\mathbf{U}) = \max_{i=j} \frac{|\mathbf{d}_i^T \mathbf{d}_j|}{\|\mathbf{d}_i\|_2 \|\mathbf{d}_j\|_2} \quad (9)$$

441 , is a measure of quality of dictionary.

442 The Internal PGs are in fact lying in the subspaces of  
 443 external PG Spaces. To defend this argument, we compare  
 444 the distribution of external PGs extracted from clean  
 445 natural images and real noisy images. For better illumination,  
 446 we randomly selected a cluster and project the original  
 447 clean PGs  $\mathbf{X}$  onto a 2-D plane. This could be done  
 448 via  $\mathbf{Xp} = \mathbf{U}(:, 1 : 2)^T \mathbf{X}$ , where  $\mathbf{U}$  is the singular vector  
 449 matrix of that cluster. The noisy PGs  $\mathbf{Y}$  assigned in this  
 450 cluster is also projected into 2-D via  $\mathbf{Yp} = \mathbf{U}(:, 1 : 2)^T \mathbf{Y}$ .  
 451 The Figure ?? reflects the distribution on the 2-D plane of  
 452 the projected clean PGs from external natural images and  
 453 the projected noisy PGs from internal image. We can see  
 454 that the internal noisy PGs are indeed lying in a subspace  
 455 of the external PGs. Hence, if we directly use the external  
 456 prior learned from clean PGs, the learned subspaces would  
 457 be too generative to be suitable for the testing data.

458 Through SVD, the PGs in each internal subspace can be  
 459 divided into singular vectors and singular values. The singular  
 460 vectors are the basis of the corresponding subspace  
 461 while the singular values reflect the importance of these basis.  
 462 The basis can be used as dictionary to code the noisy  
 463 PGs. And the singular values are adaptive parameters for  
 464 internal noisy PGs. We can compare the singular values of  
 465 one internal subspace and the corresponding space of external  
 466 PGs. The result is shown in Figure ?? . From which  
 467 we can see that the noisy subspace often have higher values  
 468 than external space consisted of clean PGs. This gap is  
 469 clearly made of the noise and can be used for image denoising  
 470 in a natural way.

## 4. The Denoising Algorithm

### 4.1. Fast Patch Group Searching by Integral Image

471 The searching of patch groups in images is inefficient  
 472 if we search non-local similar patches to each local patch.  
 473 To speed up the searching process and make our proposed  
 474 method faster, we employ the technique of 'Summed Area  
 475 Table' [36] for efficient PG searching. The SAT permits  
 476 to evaluate the sum of pixel values in rectangular regions  
 477 of the image with four operations, regardless of the region  
 478 size. That is to say, we do not need do distance measure for  
 479 each patch. It was first proposed under the name of summed  
 480 area table[37]

## 4.2. Prior Weights for Sparse Coding

486 To remove the real noise, we employ the sparse coding  
 487 framework. And in order to be adaptive to the input im-  
 488 age, we employ the internal learned  $\mathbf{U}$  of each cluster as  
 489 an adaptive dictioanry to represent the structural variations  
 490 of the PGs in that cluster. Since the  $\mathbf{U}$  is orthonormal, its  
 491 *mutual incoherence* is naturally 0 and therefore better than  
 492 other redundant dictionaries.

$$\min_{\boldsymbol{\alpha}} \|\bar{\mathbf{y}}_m - \mathbf{U}\boldsymbol{\alpha}\|_2^2 + \sum_{i=1}^{3p^2} \lambda_i |\alpha_i|. \quad (10)$$

493 The  $i$ th entry of the regularization parameter  $\lambda_i$

$$\lambda_i = \lambda / (\mathbf{S}_i + \varepsilon), \quad (11)$$

495 where  $\varepsilon$  is a small positive number to avoid dividing by zero.  
 496 Since the dictionary  $\mathbf{U}$  is orthonormal, it is not difficult to  
 497 find out that (4) has a closed-form solution (detailed deriva-  
 498 tion can be found in the supplementary material):

$$\hat{\boldsymbol{\alpha}} = \text{sgn}(\mathbf{U}^T \bar{\mathbf{y}}_m) \odot \max(|\mathbf{U}^T \bar{\mathbf{y}}_m| - \Lambda, 0), \quad (12)$$

499 where  $\Lambda = [\lambda_1, \lambda_2, \dots, \lambda_{3p^2}]$  is the vector of regulariza-  
 500 tion parameter and  $\text{sgn}(\bullet)$  is the sign function,  $\odot$  means  
 501 element-wise multiplication, and  $|\mathbf{U}^T \bar{\mathbf{y}}_m|$  is the absolute  
 502 value of each entry of vector  $|\mathbf{U}^T \bar{\mathbf{y}}_m|$ . The closed-form  
 503 solution makes our weighted sparse coding process very ef-  
 504 ficient.

## 4.3. The Overall Algorithm

505 With the solution  $\hat{\boldsymbol{\alpha}}$  in (7), the clean patch in a PG can  
 506 be estimated as  $\hat{\mathbf{x}}_m = \mathbf{D}\hat{\boldsymbol{\alpha}} + \boldsymbol{\mu}_y$ . Then the clean image  $\hat{\mathbf{x}}$   
 507 can be reconstructed by aggregating all the estimated PGs.  
 508 In practice, we could perform the above denoising proce-  
 509 dures for several iterations for better denoising outputs. In  
 510 iteration  $t$ , we use the iterative regularization strategy [38]  
 511 to add back to the recovered image  $\hat{\mathbf{x}}^{(t-1)}$  some estimation  
 512 residual in iteration  $t-1$ . The proposed denoising algorithm  
 513 is summarized in Algorithm 1 (Alg. 1).

## 5. Experiments

514 In this section, we perform real image denoising exper-  
 515 iments on three standard datasets. The first dataset is real  
 516 noisy images with mean images as ground truths provided  
 517 by [13], some samples are shown in Figure 3. The sec-  
 518 ond dataset is provided by the website of Noise Clinic [18].  
 519 The third dataset is provided by the Commercial software  
 520 Neat Image [23]. The second and third dataset do not have  
 521 ground truth images.

### 5.1. Implementation Details

522 Our proposed method contains two stages, the external  
 523 prior guided internal subspace learning stage and the adap-  
 524

540           **Alg. 1:** External Prior Guided Internal Orthogonal  
 541           Dictionary Learning for Denoising

542           **Input:** Noisy image  $y$ , PG-GMM model

543           1. Initialization:  $\hat{x}^{(0)} = y, y^{(0)} = y$ ;

544           **for**  $t = 1 : IteNum$  **do**

545            **for** each PG  $\mathbf{Y}$  **do**

546            2. Calculate group mean  $\mu_y$  and form PG  $\bar{\mathbf{Y}}$ ;

547            3. Gaussian component selection via (3);

548            **end for**

549            **for** each Internal Subspace **do**

550            4. Internal Subspace Learning by (4);

551            5. Recover each patch in all PGs via  $\hat{x}_m = \mathbf{D}\hat{\alpha} + \mu_y$ ;

552            **end for**

553            6. Aggregate the recovered PGs of all subspaces to form  
 554            the recovered image  $\hat{x}^{(t)}$ ;

555           **end for**

556           **Output:** The recovered image  $\hat{x}^{(IteNum)}$ .



557           Figure 2. Some testing images in the dataset [13].



558           Figure 3. Some cropped images of the dataset [13].

559           tive denoising stage. In the learning stage, there are 4  
 560           parameters: the patch size  $p$ , the number of patches in a PG  
 561            $M$ , the window size  $W$  for PG searching and the number of  
 562           clusters  $K$ . We set  $p = 6$  (hence the patch size is  $6 \times 6 \times 3$ ),  
 563            $M = 10$ ,  $W = 31$ ,  $K = 32$ . We extracted about 3.6 mil-  
 564           lion PGs from the Kodak PhotoCD Dataset, which includes  
 565           24 high quality color images, to train the external prior via  
 566           PG-GMM. In the denoising stage, the paramter  $\lambda = 0.002$   
 567           is used to regularize the sparse term. The  $\delta$  in iterative reg-  
 568           ularization is set as  $\delta = 0.09$ .

## 5.2. Comparison on External and Internal methods

589           In this subsection, we compared the proposed external  
 590           prior guided internal subspace learning model on real image  
 591           denoising. The three methods are evaluated on the dataset  
 592           provided in [13]. We calculate the PSNR, SSIM [21] and  
 593           visual quality of these three methods. We also compare the

594           Table 1. Average PSNR(dB)/SSIM results of external, internal,  
 595           and guided methods on 60 cropped real noisy images in [13].

	Noisy	Offline	Online	Guided
PSNR	34.51	38.19	38.07	<b>38.55</b>
SSIM	0.8718	0.9663	0.9625	<b>0.9675</b>

speed. The PSNR and SSIM results on 60 cropped images from [13] are listed in Table 1. The images are cropped into size of  $500 \times 500$  for better illustration. We also compare the three methods on visual quality in Figure 5.2. Compare the denoised images listed in Figure 5.2 and Figure 5.2, we can see that the Offline method is better at edges, smooth regions while the Online method is good at complex textures. The reason is two folds. Firstly, the Offline method is learned on clean images and hence is better at representing edges, structures, and smooth area. The online method is influenced by the noise and hence some noise cannot be removed. Secondly, the Online method is better at recovering complex area since they could learn adaptive dictionaries for the specific area. The Offline method cannot recover the complex area since they did not learn the similar structures from the external natural clean images.

## 5.3. Comparison With other Competing Methods

We compare with previous state-of-the-art Gaussian noise removal methods such as BM3D [4], WNNM [8], MLP [7], CSF [9], and the recently proposed TRD [11]. We also compare with three competing real image denoising methods such as Noise Clinic, Neat Image, and the CCNoise method proposed recently. The popular software NeatImage which is one of the best denoising software available. All these methods need noise estimation which is vary hard to perform if there is no uniform regions are available in the testing image. The NeatImage will fail to perform automatical parameters settings if there is no uniform regions.<sup>1</sup>

We the competing denoising methods from various research directions on two datasets. Both the two datasets comes from the [13]. The first dataset contains 17 images of size over  $7000 \times 5000$ . Since this dataset contains repetitive contents across different images, we crop 60 small images of size  $500 \times 500$  from these 17 images in [13].

The PSNR and SSIM resluts are listed in Table 3. The number in red color and blue color means the best and second best results, respectively. From the Table 3, we can see that the external based method can already surpass largely the previous denoising methods. The improvement on PSNR over the second best method, i.e., TRD, is 0.44dB. The

<sup>1</sup>To compare with CCNoise, we first transform the denoised images into double format.



Figure 4. Denoised images of the image "Nikon D600 ISO 3200 C1" by different methods. The images are better to be zoomed in on screen.

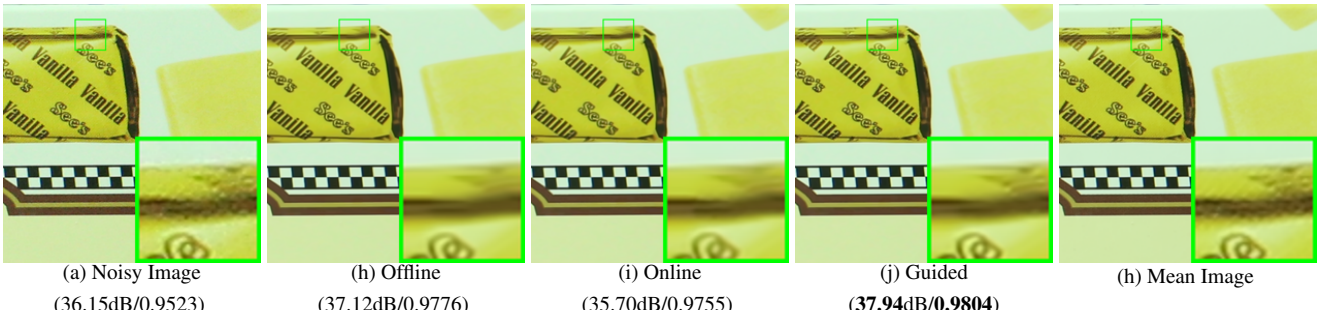


Figure 5. Denoised images of the image "Canon EOS 5D Mark3 ISO 3200 C1" by different methods. The images are better to be zoomed in on screen.

## 5.4. Discussion on Parameter $\lambda$

The proposed method only has a key parameter, namely the regularization parameters  $\lambda$ . To demonstrate that the proposed method is robust to the variance of  $\lambda$ , we vary the parameter  $\lambda$  across a wide range and obtain the PSNR and SSIM results as a function of the parameter  $\lambda$ . The results is shown in Figure 8, from which we can see that the proposed method can achieve a PSNR (SSIM) over 38.5dB (0.9660) when  $\lambda$  varies from 0.0015 to 0.0025. This shows that the proposed method is indeed robust to the chosen of the paramter  $\lambda$ .

## 6. Conclusion and Future Work

In the future, we will evaluate the proposed method on other computer vision tasks such as single image super-resolution, photo-sketch synthesis, and cross-domain image recognition. Our proposed method can be improved if we use better training images, fine tune the parameters via cross-validation. We believe that our framework can be useful not just for real image denoising, but for image super-resolution, image cross-style synthesis, and recognition tasks. This will be our line of future work.

## References

- [1] A. Buades, B. Coll, and J. M. Morel. A non-local algorithm for image denoising. *CVPR*, pages 60–65, 2005. [1](#), [2](#), [3](#)

[2] S. Roth and M. J. Black. Fields of Experts. *International Journal of Computer Vision*, 82(2):205–229, 2009. [1](#)

[3] M. Elad and M. Aharon. Image denoising via sparse and redundant representations over learned dictionaries. *Image Processing, IEEE Transactions on*, 15(12):3736–3745, 2006. [1](#), [3](#), [4](#)

[4] K. Dabov, A. Foi, V. Katkovnik, and K. Egiazarian. Image denoising by sparse 3-D transform-domain collaborative filtering. *Image Processing, IEEE Transactions on*, 16(8):2080–2095, 2007. [1](#), [2](#), [3](#), [6](#)

[5] J. Mairal, F. Bach, J. Ponce, G. Sapiro, and A. Zisserman. Non-local sparse models for image restoration. *ICCV*, pages 2272–2279, 2009. [1](#), [2](#), [3](#)

[6] D. Zoran and Y. Weiss. From learning models of natural image patches to whole image restoration. *ICCV*, pages 479–486, 2011. [1](#)

[7] Harold C Burger, Christian J Schuler, and Stefan Harmeling. Image denoising: Can plain neural networks compete with bm3d? *Computer Vision and Pattern Recognition (CVPR), 2012 IEEE Conference on*, pages 2392–2399, 2012. [1](#), [2](#), [3](#), [6](#)

[8] S. Gu, L. Zhang, W. Zuo, and X. Feng. Weighted nuclear norm minimization with application to image denoising. *CVPR*, pages 2862–2869, 2014. [1](#), [2](#), [3](#), [6](#)

[9] U. Schmidt and S. Roth. Shrinkage fields for effective image restoration. *Computer Vision and Pattern Recognition (CVPR), 2014 IEEE Conference on*, pages 2774–2781, June 2014. [1](#), [2](#), [3](#), [6](#)

Table 2. Average PSNR(dB) results of different methods on 60 cropped real noisy images captured in [13].

	Noisy	CBM3D	WNNM	MLP	CSF	TRD	NI	NC	Guided	Guided2
PSNR	34.51	34.58	34.52	36.19	37.40	37.75	36.53	37.57	38.72	38.90
SSIM	0.8718	0.8748	0.8743	0.9470	0.9598	0.9617	0.9241	0.9514	0.9694	0.9702

Table 3. Average PSNR(dB) results of different methods on 15 cropped real noisy images used in [13].

Camera Settings	Noisy	CBM3D	WNNM	MLP	CSF	TRD	NI	NC	CC	Guided2
Canon 5D Mark III ISO = 3200	37.00	37.08	37.09	33.92	35.68	36.20	37.68	38.76	38.37	40.50
	33.88	33.94	33.93	33.24	34.03	34.35	34.87	35.69	35.37	37.22
	33.83	33.88	33.90	32.37	32.63	33.10	34.77	35.54	34.91	37.13
Nikon D600 ISO = 3200	33.28	33.33	33.34	31.93	31.78	32.28	34.12	35.57	34.98	35.34
	33.77	33.85	33.79	34.15	35.16	35.34	35.36	36.70	35.95	36.69
	34.93	35.02	34.95	37.89	39.98	40.51	38.68	39.28	41.15	39.17
Nikon D800 ISO = 1600	35.47	35.54	35.57	33.77	34.84	35.09	37.34	38.01	37.99	38.82
	35.71	35.79	35.77	35.89	38.42	38.65	38.57	39.05	40.36	40.98
	34.81	34.92	34.95	34.25	35.79	35.85	37.87	38.20	38.30	38.90
Nikon D800 ISO = 3200	33.26	33.34	33.31	37.42	38.36	38.56	36.95	38.07	39.01	38.69
	32.89	32.95	32.96	34.88	35.53	35.76	35.09	35.72	36.75	36.82
	32.91	32.98	32.96	38.54	40.05	40.59	36.91	36.76	39.06	38.80
Nikon D800 ISO = 6400	29.63	29.66	29.71	33.59	34.08	34.25	31.28	33.49	34.61	33.31
	29.97	30.01	29.98	31.55	32.13	32.38	31.38	32.79	33.21	33.18
	29.87	29.90	29.95	31.42	31.52	31.76	31.40	32.86	33.22	33.35
Average PSNR	33.41	33.48	33.48	34.32	35.33	35.65	35.49	36.43	36.88	37.26
Average SSIM	0.8483	0.8511	0.8512	0.9113	0.9250	0.9280	0.9126	0.9364	0.9481	0.9505

- [10] J. Xu, L. Zhang, W. Zuo, D. Zhang, and X. Feng. Patch group based nonlocal self-similarity prior learning for image denoising. *2015 IEEE International Conference on Computer Vision (ICCV)*, pages 244–252, 2015. 1, 2, 3
- [11] Yunjin Chen, Wei Yu, and Thomas Pock. On learning optimized reaction diffusion processes for effective image restoration. *Proceedings of the IEEE Conference on Computer Vision and Pattern Recognition*, pages 5261–5269, 2015. 1, 2, 3, 6
- [12] S. J. Kim, H. T. Lin, Z. Lu, S. Ssstrunk, S. Lin, and M. S. Brown. A new in-camera imaging model for color computer vision and its application. *IEEE Transactions on Pattern Analysis and Machine Intelligence*, 34(12):2289–2302, Dec 2012. 1
- [13] Seonghyeon Nam, Youngbae Hwang, Yasuyuki Matsushita, and Seon Joo Kim. A holistic approach to cross-channel image noise modeling and its application to image denoising. *Proc. Computer Vision and Pattern Recognition (CVPR)*, pages 1683–1691, 2016. 1, 3, 5, 6, 8
- [14] J. Portilla. Full blind denoising through noise covariance estimation using gaussian scale mixtures in the wavelet domain. *Image Processing, 2004. ICIP '04. 2004 International Conference on*, 2:1217–1220, 2004. 1, 3
- [15] Tamer Rabie. Robust estimation approach for blind denoising. *Image Processing, IEEE Transactions on*, 14(11):1755–1765, 2005. 1, 3

- [16] C. Liu, R. Szeliski, S. Bing Kang, C. L. Zitnick, and W. T. Freeman. Automatic estimation and removal of noise from a single image. *IEEE Transactions on Pattern Analysis and Machine Intelligence*, 30(2):299–314, 2008. 1, 3
- [17] Zheng Gong, Zuowei Shen, and Kim-Chuan Toh. Image restoration with mixed or unknown noises. *Multiscale Modeling & Simulation*, 12(2):458–487, 2014. 1, 3
- [18] M. Lebrun, M. Colom, and J.-M. Morel. Multiscale image blind denoising. *Image Processing, IEEE Transactions on*, 24(10):3149–3161, 2015. 1, 2, 3, 5
- [19] Fengyuan Zhu, Guangyong Chen, and Pheng-Ann Heng. From noise modeling to blind image denoising. *The IEEE Conference on Computer Vision and Pattern Recognition (CVPR)*, June 2016. 1, 3
- [20] C. M. Bishop. *Pattern recognition and machine learning*. New York: Springer, 2006. 1, 3
- [21] Z. Wang, A. C. Bovik, H. R. Sheikh, and E. P. Simoncelli. Image quality assessment: from error visibility to structural similarity. *IEEE Transactions on Image Processing*, 13(4):600–612, 2004. 1, 6
- [22] K. Dabov, A. Foi, V. Katkovnik, and K. Egiazarian. Color image denoising via sparse 3d collaborative filtering with grouping constraint in luminance-chrominance space. *IEEE International Conference on Image Processing*, 1, 2007. 2
- [23] Neatlab ABSsoft. Neat image. <https://neatvideo.com/home/>. 2, 5

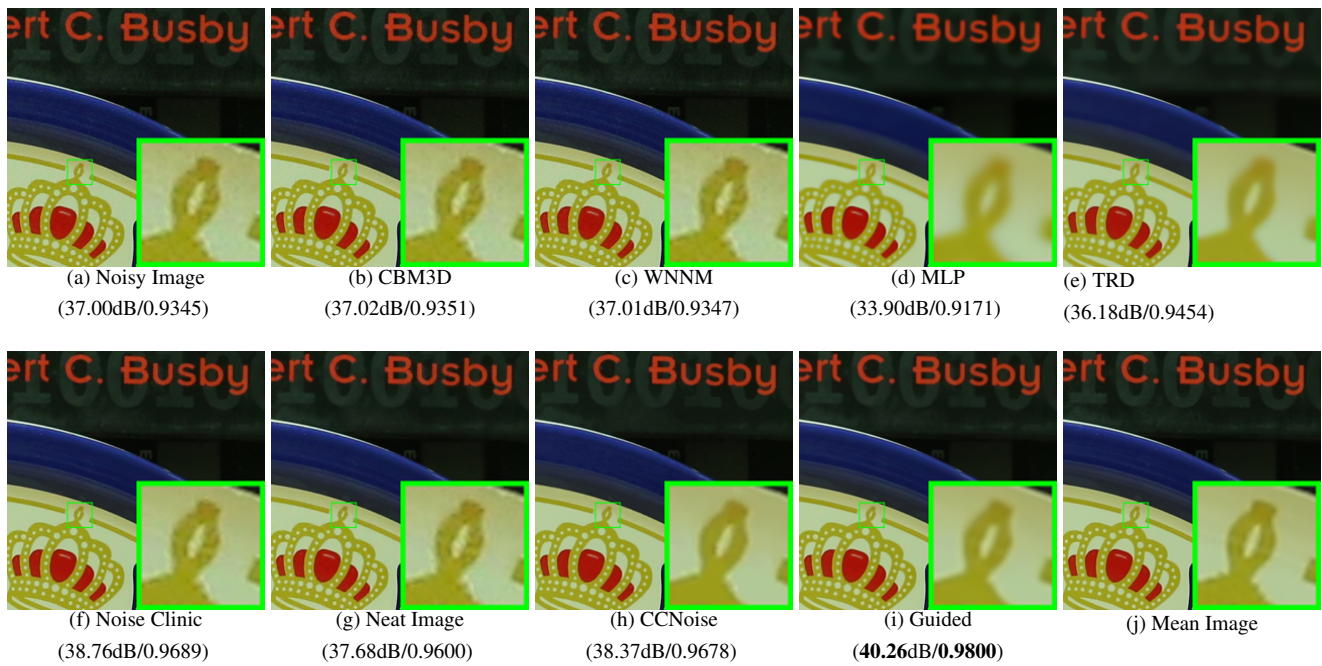


Figure 6. Denoised images of the image "Canon 5D Mark 3 ISO 3200 1" by different methods. The images are better to be zoomed in on screen.

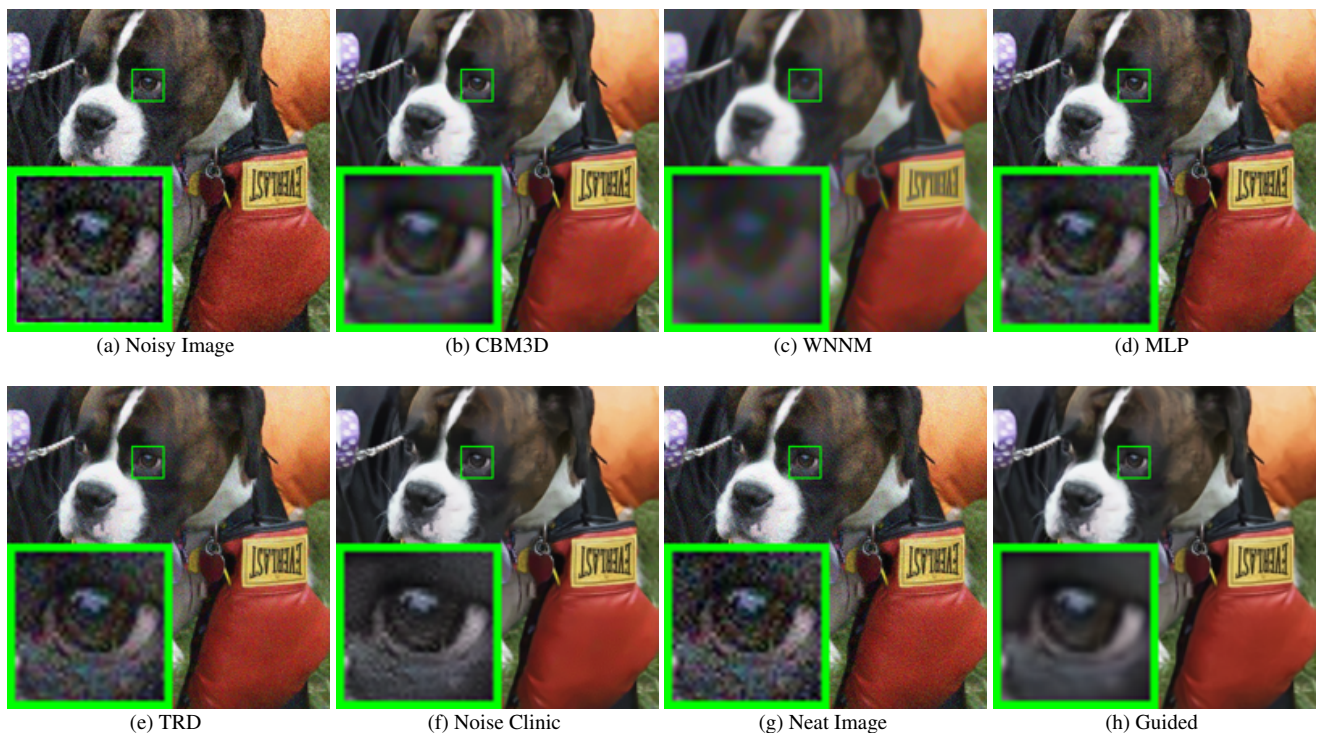


Figure 7. Denoised images of the image "5dmak3iso32003" by different methods. The images are better to be zoomed in on screen.

[24] Glenn E Healey and Raghava Konddepudy. Radiometric ccd camera calibration and noise estimation. *IEEE Transactions on Pattern Analysis and Machine Intelligence*, 16(3):267–276, 1994. 1, 3

[25] Daniel Glasner, Shai Bagon, and Michal Irani. Super-resolution from a single image. *ICCV*, 2009. 3

[26] Maria Zontak, Inbar Mosseri, and Michal Irani. Separating signal from noise using patch recurrence across scales. *Pro-*

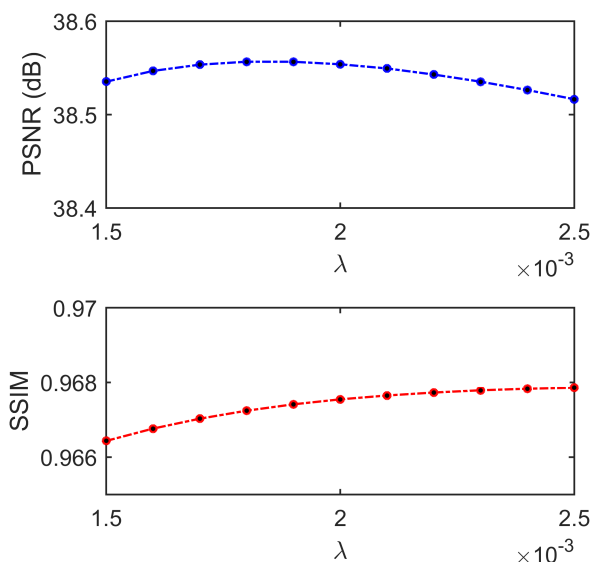


Figure 8. The PSNR/SSIM results as a function of the parameter  $\lambda$ .

*ceedings of the IEEE Conference on Computer Vision and Pattern Recognition*, pages 1195–1202, 2013. 3

- [27] Tomer Michaeli and Michal Irani. Blind deblurring using internal patch recurrence. *European Conference on Computer Vision*, pages 783–798, 2014. 3
- [28] Y. Bahat and M. Irani. Blind dehazing using internal patch recurrence. *IEEE International Conference on Computational Photography (ICCP)*, pages 1–9, May 2016. 3
- [29] J. Portilla, V. Strela, M.J. Wainwright, and E.P. Simoncelli. Image denoising using scale mixtures of Gaussians in the wavelet domain. *Image Processing, IEEE Transactions on*, 12(11):1338–1351, 2003. 3
- [30] Peter J Huber. *Robust statistics*. Springer, 2011. 3
- [31] M. Lebrun, A. Buades, and J. M. Morel. A nonlocal bayesian image denoising algorithm. *SIAM Journal on Imaging Sciences*, 6(3):1665–1688, 2013. 3
- [32] W. Dong, L. Zhang, G. Shi, and X. Li. Nonlocally centralized sparse representation for image restoration. *Image Processing, IEEE Transactions on*, 22(4):1620–1630, 2013. 3
- [33] Chenglong Bao, Jian-Feng Cai, and Hui Ji. Fast sparsity-based orthogonal dictionary learning for image restoration. *Proceedings of the IEEE International Conference on Computer Vision*, pages 3384–3391, 2013. 4
- [34] A. P. Dempster, N. M. Laird, and D. B. Rubin. Maximum likelihood from incomplete data via the EM algorithm. *Journal of the Royal Statistical Society. Series B (methodological)*, pages 1–38, 1977. 5
- [35] David L Donoho and Michael Elad. Optimally sparse representation in general (nonorthogonal) dictionaries via 1 minimization. *Proceedings of the National Academy of Sciences*, 100(5):2197–2202, 2003. 5

- [36] Franklin C. Crow. Summed-area tables for texture mapping. *SIGGRAPH Comput. Graph.*, 18(3):207–212, January 1984. 5
- [37] Paul Viola and Michael J Jones. Robust real-time face detection. *International journal of computer vision*, 57(2):137–154, 2004. 5
- [38] S. Osher, M. Burger, D. Goldfarb, J. Xu, and W. Yin. An iterative regularization method for total variation-based image restoration. *Multiscale Modeling & Simulation*, 4(2):460–489, 2005. 5